YALE PEABODY MUSEUM

P.O. BOX 208118 | NEW HAVEN CT 06520-8118 USA | PEABODY.YALE. EDU

Journal of Marine Research

The *Journal of Marine Research,* one of the oldest journals in American marine science, published important peer-reviewed original research on a broad array of topics in physical, biological, and chemical oceanography vital to the academic oceanographic community in the long and rich tradition of the Sears Foundation for Marine Research at Yale University.

An archive of all issues from 1937 to 2021 (Volume 1–79) are available through EliScholar, a digital platform for scholarly publishing provided by Yale University Library at https://elischolar.library.yale.edu/.

Requests for permission to clear rights for use of this content should be directed to the authors, their estates, or other representatives. The *Journal of Marine Research* has no contact information beyond the affiliations listed in the published articles. We ask that you provide attribution to the *Journal of Marine Research.*

Yale University provides access to these materials for educational and research purposes only. Copyright or other proprietary rights to content contained in this document may be held by individuals or entities other than, or in addition to, Yale University. You are solely responsible for determining the ownership of the copyright, and for obtaining permission for your intended use. Yale University makes no warranty that your distribution, reproduction, or other use of these materials will not infringe the rights of third parties.

Spatial continuity of measured seawater and tracer fluxes through Nares Strait, a dynamically wide channel bordering the Canadian Archipelago

by Andreas Münchow[1], Kelly K. Falkner[2] and Humfrey Melling[3]

ABSTRACT

Freshwater delivered as precipitation and runoff to the North Pacific and Arctic oceans returns to the Atlantic principally via the Canadian polar shelf and Fram Strait. It is conveyed as ice or freshened seawater. Here we use detailed ship-based measurements to calculate a snap-shot of volume, freshwater, and tracer fluxes through Nares Strait, a 500-km long waterway separating Greenland and Ellesmere Island. We use quasi-synoptic observations of current by ship-mounted acoustic Doppler current profiler (ADCP), of salinity and temperature by CTD probe and of dissolved nutrients by rosette bottle sampler on four cross-sections between 82 and 78N latitude. Data were collected during the first half of August 2003. We partition the fluxes into components derived from Pacific and Atlantic inflows into the Arctic Ocean. During the time of the survey, there was a net southward 0.91 ± 0.10 Sv (10^6 m^3 s^{-1}) flux of volume and a net southward 31 ± 4 10^{-3} Sv (977 ± 127 km^3 y^{-1}) flux of freshwater relative to a salinity of 34.8. Much of the volume flux was carried within a strong (40 cm s^{-1}), narrow (10 km) subsurface jet hugging the western (Ellesmere Island) side of the strait. The presence of this jet in four sections spanning the 500-km length of the strait is evidence of a buoyant boundary current through the strait. The jet was coincident with elevated concentrations of phosphate (1.0 mmol m^{-3}) and silicate (11 mmol m^{-3}) which both indicate a Pacific Ocean source. We interpreted the ratio of dissolved total inorganic nitrogen to phosphate in terms of fractional dilution of Atlantic by Pacific waters. About 0.43 ± 0.10 Sv (39%) of the southward flow was of Pacific origin. These results are a snapshot during the summer of 2003 following a prolonged period of northward directed wind stress when ice cover was mobile. Although long-term mean values are likely different, we determined that the major fraction of the through-flow is carried by a jet of scale determined by the internal Rossby radius (5-10 km).

1. Introduction

Nineteen ship-wrecked members of the Polaris expedition of 1871-72 drifted on ice floes a distance of over 2500 km from Nares Strait near 79N latitude to Newfoundland. Surviving this six-month-long ordeal, they inadvertently mapped for the first time a drift of icy waters from the Arctic to the North Atlantic Ocean. That they survived to tell the tale is

1. College of Marine and Earth Studies, University of Delaware, Newark, Delaware, 19716, U.S.A. *email: muenchow@udel.edu*
2. College of Oceanic and Atmospheric Sciences, Oregon State University, Corvallis Oregon, 97331, U.S.A.
3. Institute of Ocean Sciences, Sidney, BC, Canada, V8L 4B2.

tribute to two Inuit, Joe Ebierbing and Hans Hendrik, whose hunting skills and diligence provided food for the entire party (Hendrik, 1878). Almost a century later, 1962-64, ice island WH-5 was carefully tracked via ships and aircraft from north of Ellesmere Island (83N) to the Atlantic via Nares Strait (Nutt, 1966). The movements of ice and water so revealed are one link in the global hydrological cycle whose significance to global climate has yet to be understood. Neither our physical understanding nor our knowledge of fluxes is sufficient for useful incorporation of this marine element into the numerical simulations of climate that are in common use in the prediction of future climate.

In the global hydrologic cycle, the Arctic Ocean is the conduit for return of water evaporated from the subtropical Atlantic and delivered as precipitation and runoff to the North Pacific and Arctic oceans. The Arctic Ocean receives run-off from Eurasia and North America (about 10% of global river flow), a low salinity inflow through Bering Strait that is a freshwater source of half this magnitude (Aagaard and Carmack, 1989) and a surplus of precipitation over evaporation. Freeze-thaw cycles and mixing modify the imprint of these freshwater sources within the Arctic before they return to the North Atlantic in the guise of ice or diluted seawater, principally through the Canadian Archipelago and Fram Strait (Serreze *et al.*, 2006).

Impacts of variable freshwater export from the Arctic have been observed in the Greenland and Labrador seas where North Atlantic deep waters are formed: the Great Salinity Anomaly spreading over the North Atlantic since 1970 (Belkin *et al.*, 1998) and a more recent freshening and warming of deep waters (Curry and Mauritzen, 2005; Dickson *et al.*, 2002; Rhein *et al.*, 2002; Zweng and Münchow, 2006). Models and observations link the propagation of these signals to atmospheric variations (Dickson *et al.*, 1996; Weaver *et al.*, 1994; Wohlleben and Weaver, 1995). Furthermore, models predict that increased surface freshening and warming in the Greenland and Labrador seas will slow global overturning of the oceans (Delworth and Dixon, 2000; Rahmstorf and Ganopolski, 1999). Possible early evidence for such slowing has been recently reported (Bryden *et al.*, 2005), although Wunsch and Heimbach (2006) have argued that apparent trends may be a consequence of aliasing.

Estimates of flux contributions from the Arctic via various pathways indicate that the two principal components are those bracketing Greenland and that these two flows are of roughly equal size. Dickson *et al.* (2007) have concluded that flows via both routes are unsteady and that the overturning circulation is not equally sensitive to both. For example, a reanalysis of HadCM3 results at the UK Meteorological Office has shown that the impact of an increased freshwater outflow on the overturning depends on whether it was distributed over depth in the north-west Atlantic or simply spread across the surface (Vellinga, 2005). While the flux east of Greenland can be carried to depth via the dense overflow from Nordic Seas (Dickson *et al.*, 2002), the flux through the Archipelago cannot. Hence the delivery point of freshwater flux is important. Recent model runs predict that the increase in the Arctic efflux of ice and freshwater by 2070-99 is likely to be greater for the

Canadian Archipelago (+48%) than for Fram Strait (+3%) (H. Haak, personal communication).

Most flow across the Canadian polar shelf between the Arctic and the Atlantic passes via three pathways, Parry Channel with sill limiting through-flow to 125-m depth (Prinsenberg and Hamilton, 2005), Cardigan Strait with a 180-m sill, and Nares Strait with a 220-m sill. The deepest of these sills coincides with the depth of the 34.65 isohaline in adjacent waters of the Canada Basin. Melling (2000) reviewed knowledge of the Canadian Arctic through-flow in relation to the freshwater budget of the Arctic. The immediate recipient of freshwater passing through the Archipelago is Baffin Bay, a deep (2400 m) basin bordered by banks. Baffin Bay is in turn connected to the Labrador Sea by a 675-m sill in Davis Strait. Fluxes of volume and especially freshwater through any of these channels and straits are rarely measured directly at the dynamically relevant scale, i.e., the internal Rossby radius of deformation

$$L_D \sim (g \; \Delta\rho/\rho_0 D)^{1/2}/f$$

which in our study area is ~10 km. Here g~9.81 m s^{-2} is the constant of gravity, $\Delta\rho$~2 kg m^{-3} is a characteristic density difference, ρ_0 ~1027 kg m^{-3} is an ambient density, D~100 m is a vertical scale of motion, and f~1.44×10^{-4} s^{-1} is the Coriolis parameter. Münchow *et al.* (2006) present the first synoptic velocity observation from a single section in Nares Strait and find that this scale matches both the spatial extent of observed sloping isopycnals as well as spatial velocity features in geostrophic thermal wind balance. We here extend this study by investigating the along-channel continuity and composition of the generally southward flux of volume, freshwater, and tracers along the 500 km long Nares Strait.

2. Data sources and methodology

The USCGC *Healy* supported wide ranging oceanographic observations between 78 and 83N latitude in Nares Strait during August 2-14 2003 (Fig. 1). We here discuss data from (a) surveys that utilized continuous underway acoustic Doppler current profiling (via ship-mounted ADCP), (b) frequent stations where vertical hydrographic profiles were measured by conductivity-temperature depth probe (CTD), and (c) water sampling rosette. In addition, we use time series data retrieved from instruments moored in the strait in August 2003 by USCGC *Healy* and recovered in August 2006 by CCGS *Henry Larsen*.

The USCGC *Healy* carries a 75-kHz phased-array ADCP (Ocean Surveyor) mounted under the hull to measure depth profiles of horizontal current. Attitude information (heading, pitch, roll) is provided by an Ashtech ADU2-3DGPS receiver while position is derived from a Trimble Centurion p-code DGPS system. These data streams provide earth-referenced horizontal current at depths between about 20 m and the seabed or 400 m, whichever is less. In the Appendix we discuss how we process noisy ADCP data in ice-infested Arctic waters, their calibration, the removal of deterministic tidal currents as well as spatial averaging and extrapolation. These are critical quality control issues as our
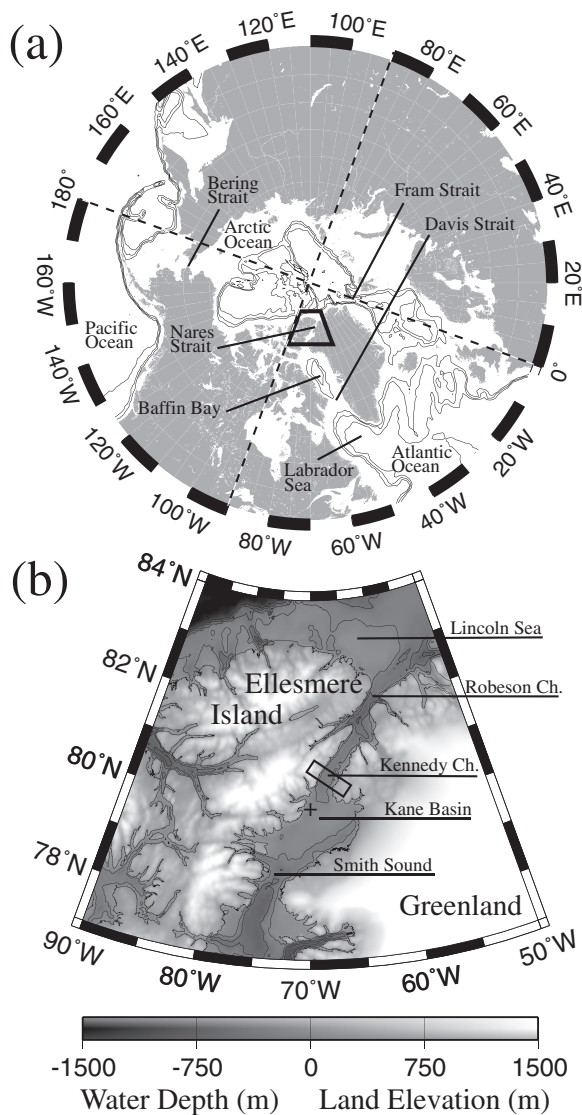
Figure 1. Map of the study area (a) northern hemisphere and (b) Nares Strait where the rectangle indicates the location of the mooring array and the "+" symbol indicates the location of the 220-m deep sill. Contours are bathymetry with intervals of 1000-3000 m in (a) and 250-1000 m in (b).

data originate from a region where ADCP velocity data are uncommon, frequently misinterpreted, and often regarded with either discomfort or skepticism.

The CTD rosette carried by USCGC *Healy* uses an SBE 9+ system (Sea Bird Electronics) with duplicate conductivity (SBE-4C) and temperature (SBE-3+) sensors and

a single Paroscientific Digiquartz pressure sensor. Temperature and conductivity sensors were calibrated in 2003 and the pressure sensor in 2001.

The salinity of sampled water was determined at sea after its equilibration over 12 hours to room temperature; the salinometer (Guildline Autosal 8400 B) was operated in a temperature controlled room. Results are accurate to ± 0.001 (PSS78). Nutrient concentrations were determined at sea following the JGOFS/WOCE suggested protocols (Gordon *et al.*, 1994). The short-term precision of the nutrient analyses is typically 0.2% for Si, 0.4% for PO_4, 0.3% for NO_3^-, 0.02 mmol/m^3 NO_2^-, and 0.03 mmol m^{-3} for NH_4^+. However, the inter-cruise reproducibility achieved during the WOCE Hydrographic Program, Pacific One-Time Survey for Si, PO_4^{3-}, and NO_3^- was larger reaching 1%, 2%, 1%, respectively (unpublished data, Ross *et al.*).

There are no locations along Nares Strait where wind is measured. Moreover, airflow is strongly channeled by high terrain. To determine winds prior to and during our survey we have used predictions from the high-resolution, nested, three-dimensional MMP-5 numerical model configured for this area (Samelson *et al.*, 2006). The model correctly predicted ageostrophic hurricane-strength winds during the evacuation of an ice camp in April 2005 (Samelson and Barbour, 2008). Model winds correlated strongly with along-channel pressure gradients suggested by coastal atmospheric surface pressure observations to the north and south of Nares Strait (Samelson *et al.*, 2006). Such a correlation strongly suggests ageostrophic atmospheric motions inside the channel.

To provide temporal context we have used preliminary current records from two bottom-mounted 75-kHz ADCPs retrieved in August 2006. The ADCPs returned data at 8-m increments between 15 m above the seafloor to 20 m below the sea surface; data were recorded every 30 minutes for three years. Because a magnetic compass is an unreliable heading reference close to the magnetic pole, we developed a novel torsionally rigid mooring that has the capability to pitch and roll in response to the force of current but not to swivel. Hence the heading of the instrument is fixed (but unknown) during its deployment. The heading is determined from the data record a posteriori via a vector-correlation analysis of barotropic tidal current predictions (Padman and Erofeeva, 2004) and depth-averaged tidal currents from the moored instrument. This procedure works well in Kennedy Channel because the dominant semi-diurnal tidal currents are rectilinear (Münchow *et al.*, 2006; Padman and Erofeeva, 2004) and intermittent tidal variability is weak. The direction of depth-averaged three-year average flow is aligned along-channel to within 2°.

3. Flows and fluxes

We focus on the continuity of the subtidal flow through four reference sections along Nares Strait. The northernmost is across northern Robeson Channel at 82N, the southernmost is across southern Smith Sound at 78N and the other two are in Kennedy Channel, one across its northern end at 81N and the other across the southern end at 80° 30'N (see Fig. 1).
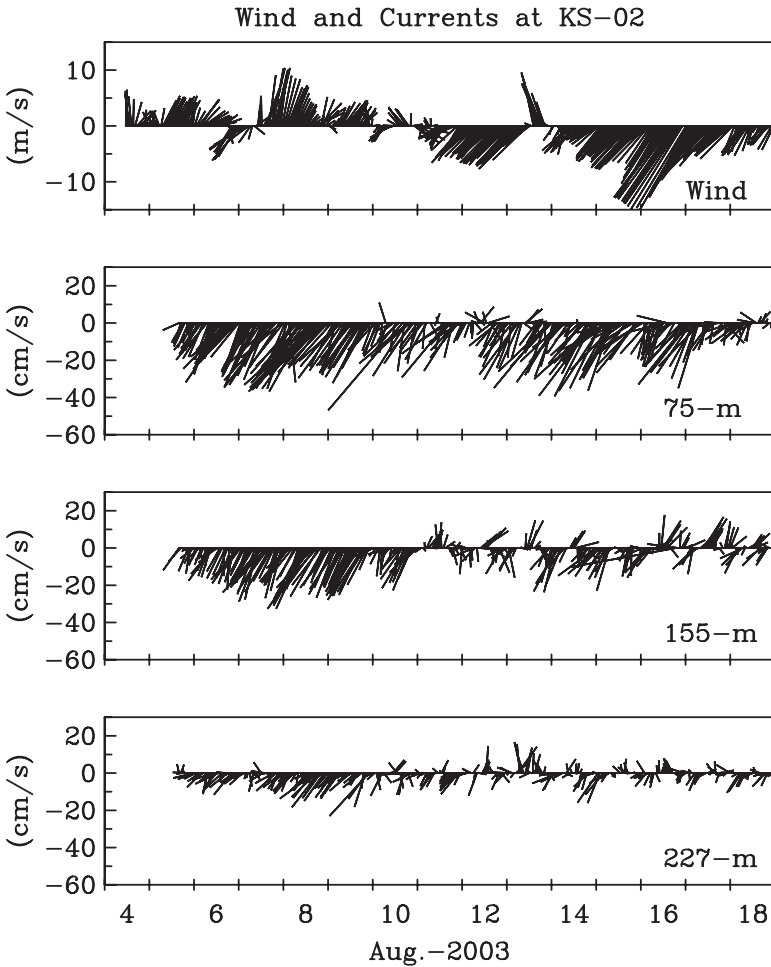
Figure 2. Time series of surface wind forcing (top panel) and de-tided currents from the western side of southern Kennedy Channel off Canada (KS-02) at three different depths representing near-surface (75 m; z/H~0.25), mid-depth (155 m; z/H~0.5), and near-bottom (227 m; z/H~0.75) currents.

a. Time series in Kennedy Channel

During the period of velocity and tracer surveys in Nares Strait (2-15 August 2003) a line of instrumented moorings was deployed across southern Kennedy Channel. In Figure 2 and Figure 3 we show current measured by ADCP within 2 km of the Ellesmere and Greenland sides of the strait. Time series are shown for levels at one quarter, half and three quarters (z/H of 0.25, 0.5, 0.75) of the local depth H, which was 299 m near Ellesmere (site KS-02) and 154 m near Greenland (KS-14). Figure 2 and Figure 3 span the two weeks of our surveys in 2003; the values are unfiltered, but the deterministic tidal component
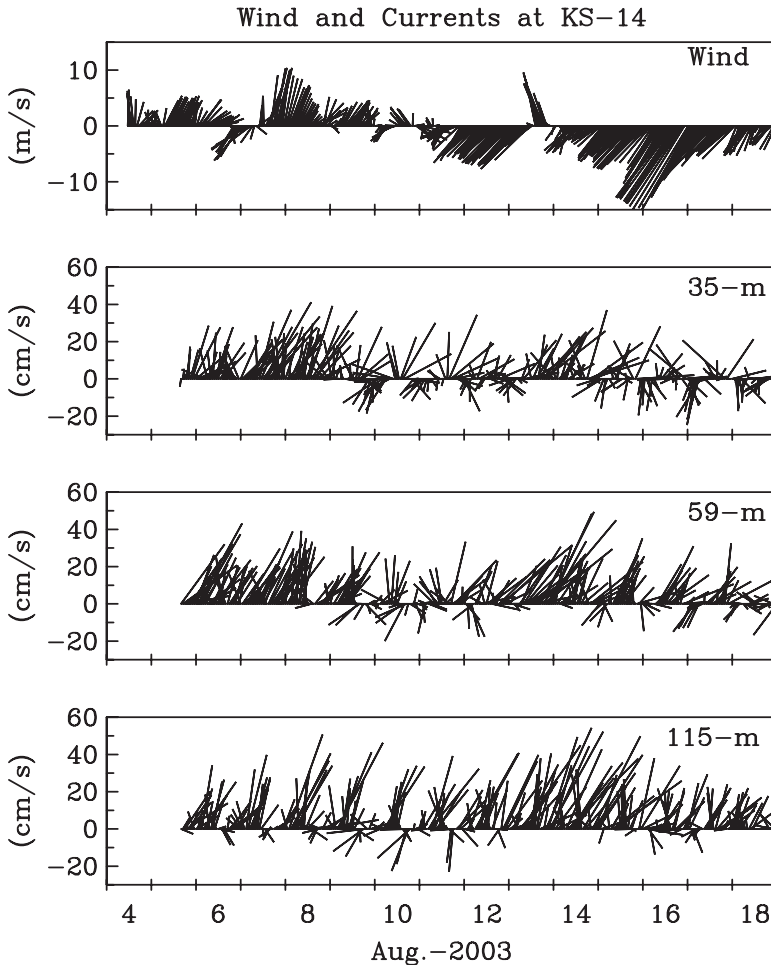
Figure 3. As Figure 2, but for the eastern side of Kennedy Channel off Greenland (KS-14).

determined by harmonic analysis of the three-year record (M_2, S_2, N_2, K_2, K_1, O_1 constituents) has been removed. Note the residual diurnal component persists in the de-tided records. The time series of surface wind is that predicted by the model of Samelson *et al.* (2006).

Near Ellesmere (Fig. 2; KS-02) there was a persistent southward flow at about 30 cm s^{-1} over the central half of the water column that ran counter to the local wind for much of the time. Strangely, when the wind reversed direction on August 11 to blow down the channel in the direction of the currents, the down-channel current actually weakened. The relationship between wind and current off the coast off Greenland 30 km away (Fig. 3; KS-14) was similarly disconnected, despite the average flow direction being downwind here. When the wind changed on August 11 to oppose the northward current the flow

actually strengthened. The speeds of the southward flow off Canada and the northward flow off Greenland both increase as the local winds opposing them increase, implying that the lateral shear in current changes little with change in flow strength. We cannot explain this curious feature of the oceanic flow, however, we speculate that a subtle arrangement or baroclinic and barotropic pressure gradient in ageostrophic balance may reveal the the underlying dynamics as the channel contains steep sidewalls and is dynamically wide enough to allow both barotropic and baroclinic pressure gradients (Münchow *et al.*, 2006). Propagating baroclinic wave motions (Johnson and Garrett, 2006) are another dynamic possibility. In order to test these speculations, a more systematic statistical analysis of the entire 3-year record is required. This is beyond the scope of the present discusion that focuses on the continuity of sectionally averaged flux estimates along the the 500-km long Nares Strait.

b. *Cross-section of Robeson Channel*

Robeson Channel connects the Lincoln Sea to Hall Basin. It is about 60-km long, 30-km wide and more than 400-m deep along its axis. Figure 4 shows the location and the along-shore flow at 101-m depth as a composite of observations collected between 02:48 UTC August 8 and 05:21 UTC August 10 2003. Adjacent to the coast of Ellesmere Island we measured a southward flowing, wall-bounded jet that was 10-km wide, had a peak speed in excess of 40 cm s^{-1} and extended to depth greater than 300 m (Fig. 5). The high speed core appeared between 100-m and 200-m depth within 3 km of the Ellesmere coast. During the weeks before the survey, persistent upwelling-favorable winds may have weakened southward flow in the upper 50-100 m off Ellesmere Island. The flow through the eastern two thirds of the section was weak, with the exception of a 20 cm s^{-1} southward flow above 50-m depth near mid channel and an underlying 10 cm s^{-1} northward flow below 350 m. The explanation of these features is not obvious.

This snapshot is consistent with measurements by current meters moored in Robeson Channel for six weeks in the late winters of 1971 and 1972 (Sadler, 1976; Godin, 1979). At 5 km from Ellesmere Island, these data revealed average southward flow at 40 cm s^{-1} at 100 m decreasing to 20 cm s^{-1} near the seabed at 650 m and to less than 10 cm s^{-1} at 5-m depth beneath land-fast ice. At mid-channel the current was less than 15 cm s^{-1} southward at 100 m. There was a weak northward average current at 100-m depth 5 km off the Greenland coast. The uncharacteristically strong southward current measured by one of Sadler's instrument at 100-m depth in 1971 was often questioned, however, these suspicions were probably unwarranted.

Integration of the along-channel speed across the section provides the net volume flux, about -0.77 Sv (10^6 m^3/s) (Table 1) with separate southward and northward components of -0.96 Sv and +0.19 Sv, respectively. The spatial separation of northward and southward flows through the section suggests that the component fluxes may involve seawater of different origin. We now proceed to discriminate between a fresher and colder unit that is
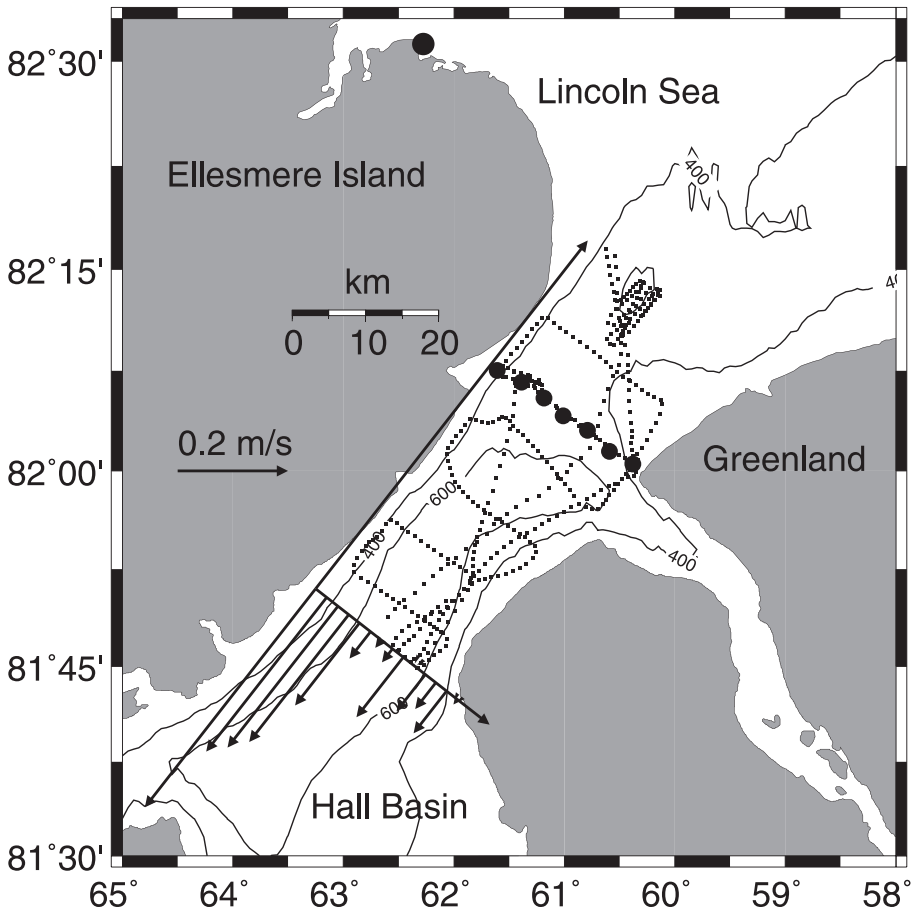
Figure 4. Along-channel currents at 101-m depth of Robeson Channel from ADCP surveys. Small
    dots are ADCP data locations while the thick circles indicate hydrographic stations.

dominated by waters from the Pacific Ocean and a saltier and warmer unit that is traceable
to the Atlantic.

Concurrent hydrographic measurements permit an analysis that utilizes measured
concentrations of dissolved phosphate (PO_4^{3-}) and total inorganic nitrogen (TIN) to
determine the relative magnitudes of Pacific and Atlantic influence. TIN is the sum of
nitrate (NO_3^-), nitrite (NO_2^-) and ammonium (NH_4^+). Pacific waters entering the Arctic via
Bering Strait are stripped of some of their fixed nitrogen via de-nitrification as they cross
the biologically productive shelves of the Bering and Chukchi seas. In contrast Atlantic
waters enter the Arctic via the deeper waters of Fram Strait and the Barents Sea and are not
measurably impacted by denitrification. Both water types are then subject to "Redfield"
production and respiration that affects their nutrient content in roughly fixed ratios. Hence,
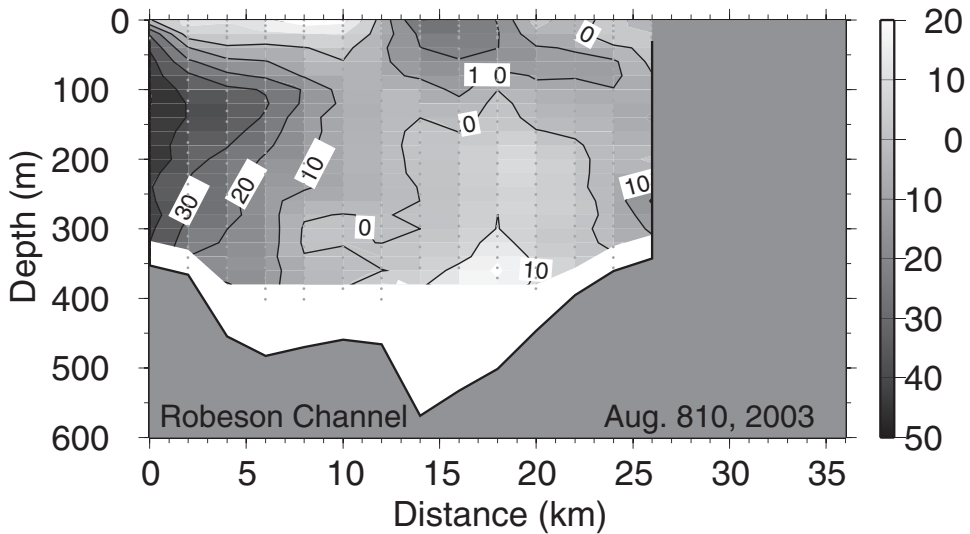
Figure 5. Along-channel velocity section across Robeson Channel from Ellesmere Island on the left to Greenland on the right. Dark shades indicate negative, that is, southward flow (see Fig.3 for data locations).

the different histories of Pacific and Atlantic inflows to the Arctic create two distinct linear correlations between TIN and PO_4 (Jones *et al.*, 1998; Yamamoto-Kawai *et al.*, 2008). Hence a measured value of TIN will lie between two PO_4 calculated from known Pacific and Atlantic TIN vs. PO_4 regression lines. The fraction of Pacific waters f_{PW} is then estimated from the measured PO_4 value, P_{obs} and predicted PO_4 values for pure Pacific, P_{PW} and Atlantic, P_{AW}, waters as $f_{PW} = P_{obs}/(P_{PW} + P_{AW})$. Runoff from rivers will dominantly add to the Atlantic fraction, because riverine nutrient ratios are closer to the Atlantic than the Pacific endmembers (Taylor *et al.*, 2003).

Table 1. Nares strait fluxes (negative southward).

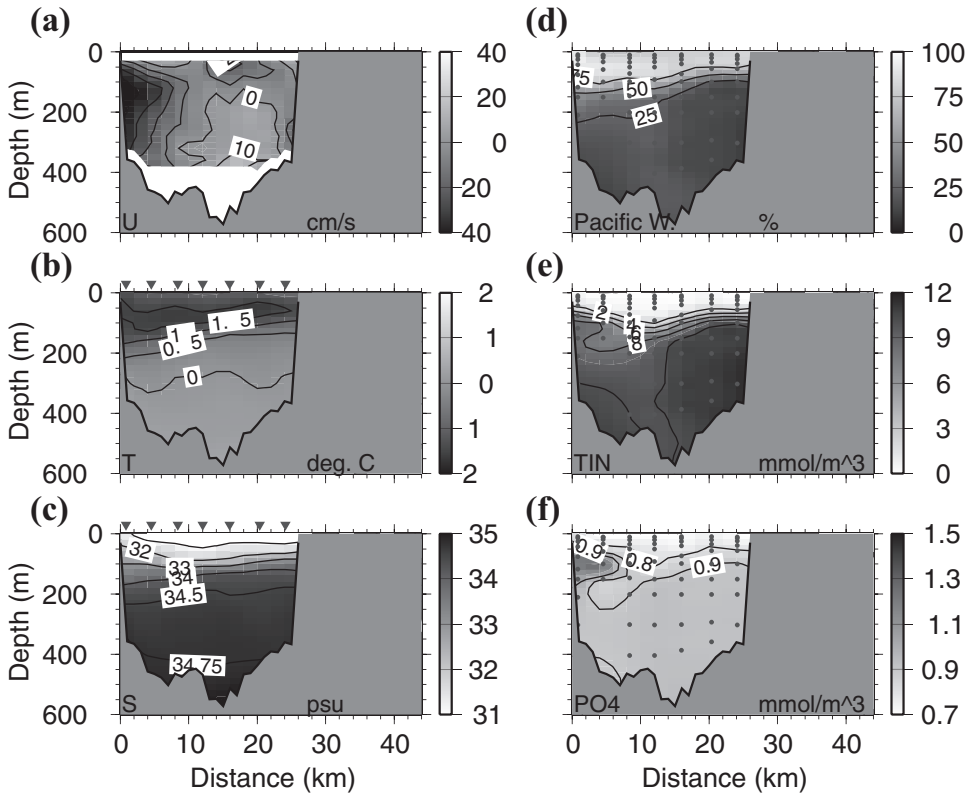| Location	Net volume flux (Sv)	Net Atlantic W. flux (Sv)	Net Pacific W. flux (Sv)	Net freshwater flux (10^{-3} Sv)	Along-channel wind (m/s)	Data (days)
Robeson	−0.77	−0.40	−0.37	−25.8	+11.6	2.10
Kennedy-N	−0.92	−0.61	−0.31	−30.9	+5.6	0.88
Kennedy-S	−0.91	−0.65	−0.26	−30.4	+2.5	2.23
Smith Sound	−1.03	−0.70	−0.33	−34.5	+2.1	0.92
Average	−0.91 ± 0.10	−0.59 ± 0.13	−0.32 ± 0.04	−31 ± 4		
Regression, no wind	−1.03 ± 0.10	−0.75 ± 0.05	−0.28 ± 0.06	−34 ± 3		

Figure 6. Robeson Channel section data of (a) along-channel velocity, (b) potential temperature, (c) salinity), (d) percent Pacific water that is calculated from (e) total inorganic nitrogen (TIN), and (f) phosphate (PO_4) distributions. Symbols indicate hydrographic stations.

Figure 6 shows the distribution of Pacific water, tracer concentration, temperature, salinity and flow speed across the Robeson Channel section. The temperature and salinity sections within 12 km of Canada have contours sloping upward toward Ellesmere above 200 m and downward below 200 m. Hence baroclinic structure in the density field (not shown as it closely mimics salinity) explains part of the southward flow. There is a clear coincidence of the current jet with maxima in dissolved nutrient concentration, particularly phosphate and silicate (not shown) at 100-m depth within 8 km of Ellesmere Island (Fig. 6), as discussed previously by Falkner *et al.* (2008). This compact feature is superposed on a general plunging of isolines in all properties towards Canada. The relatively fresh, cold, nutrient-depleted Pacific waters occupy a 100-m thick near-surface layer off Ellesmere Island which thins to 50 m off Greenland. The southward moving Pacific water is a freshwater source for Baffin Bay that we will subsequently trace along the full length of Nares Strait.

We estimate fluxes of seawater properties, F_ψ, by multiplying tracer concentration, ψ and along-channel current, u and integrating the product over the cross-section ($\delta x, \delta z$):

$$F_\psi = \int\int \psi u \delta x \delta z.$$

If $\psi = 1$ the result is the net volume flux (-0.77 Sv). If $\psi = PW$ (Pacific water fraction) then the result is the volume flux of Pacific water, about -0.37 Sv (Table 1) while for $\psi = AW$ (Atlantic water fraction) we obtain the volume flux of Atlantic water, about -0.40 Sv. Separating the fluxes into northward and southward components by integrating positive and negative values of (ψu), we find that 55% and 45% of the 0.96 Sv southward transports are associated with Atlantic and Pacific waters, respectively. For the much smaller 0.19 Sv northward transport 68% are of Atlantic and 32% are of Pacific origin (Table 1).

If $\psi = (1 - S/34.8)$, we calculate a freshwater flux relative to 34.8 salinity, which is about $26 \cdot 10^{-3}$ Sv (Table). The net freshwater flux through Robeson Channel is about 7% of the net Pacific water volume flux, a similar value to the 9% estimated by Jones and Eert (2006) who used assumed bulk values for Atlantic and Pacific salinity in the Arctic and for Bering Strait and fluvial volume flux entering the Arctic Ocean.

The southward flux of dissolved nutrient through Nares Strait passes into the North Water polynya in northern Baffin Bay. Here the Arctic outflow may deliver nutrients to support the high primary productivity of the polynya. For $\psi = PO_4$ (phosphate, P) we calculate a net flux of -580 mole s^{-1}, which could provide up to 0.6 mmole m^{-2} d^{-1} (60 mg-P m^{-2} d^{-1}), if uniformly accessible to plankton over an area of 8×10^4 km^2. For $\psi = H_2SiO_3$ (silicic acid, Si) the advective flux is about -6,800 mole s^{-1} corresponding to 7 mmole m^{-2} d^{-1} (550 mg-Si m^{-2} d^{-1}). However, since these fluxes are carried primarily by the velocity core at 100-m depth, they are not necessarily accessible to primary production occurring in the much shallower photic zone in the polynya (Melling *et al.*, 2001).

Robeson Channel opens southward into Hall Basin with Lady Franklin Bay to the west and Petermann Fjord to the east. We lack current data for the 10-km wide Lady Franklin Bay, but freshwater inputs here are probably minor as its watershed is small without a major connection to the Ellesmere Island ice sheets. We have ADCP and CTD data for the 15-km wide Petermann Fjord, fed by a major outlet of the Greenland icecap, Petermann Glacier. Nonetheless, despite a 30 m s^{-1} outflow catabatic wind event during our survey, our ADCP observations (not shown) indicate a negligible volume flux (0.06 Sv) into Hall Basin, less than 10% of the Nares Strait flux and within the uncertainty of our measurements.

c. *Cross-sections of Kennedy Channel*

Sections were occupied at both the northern and southern end of Kennedy Channel. The strongest southward flow at 101-m depth was about 20 cm s^{-1}, down from 40 cm s^{-1} measured in Robeson Channel; however, the overall width of the south-going stream at this
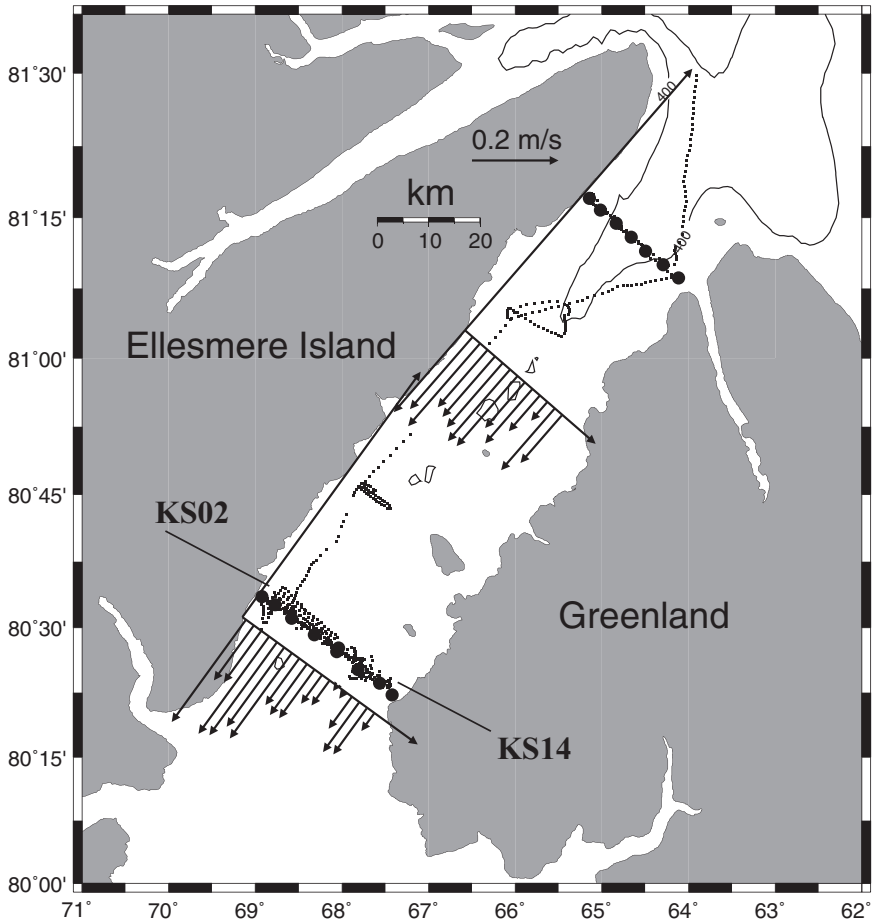
Figure 7. As Figure 4, but for Kennedy Channel. Northern and southern sections are constructed from data north and south of 81N. Small dots indicate ADCP data, large circles indicate hydrographic stations. Mooring locations KS02 and KS14 are indicated near the two inshore CTD casts off Ellesmere Island and Greenland, respectively. Coordinate systems are indicated by long arrows anchored to a coastal point on Ellesmere Island.

depth appears wider here (Fig. 7). Cross-sections of flow speed and hydrographic structure within Kennedy Channel are shown in Figure 8 and Figure 9; the channel widens from 26 km to 36 km and shoals from 400 m to 300 m depth between the northern and southern sections. For salinity greater than 33.5, isolines slope steeply downward within 10 km off Ellesmere Island coincident with the zone of strongest current. Fresher isohalines slope upward but more gently, perhaps indicating an internal response to prevailing up-channel wind stress for several weeks before the survey. There is no evidence of a northward flow at depth on the Greenland side.
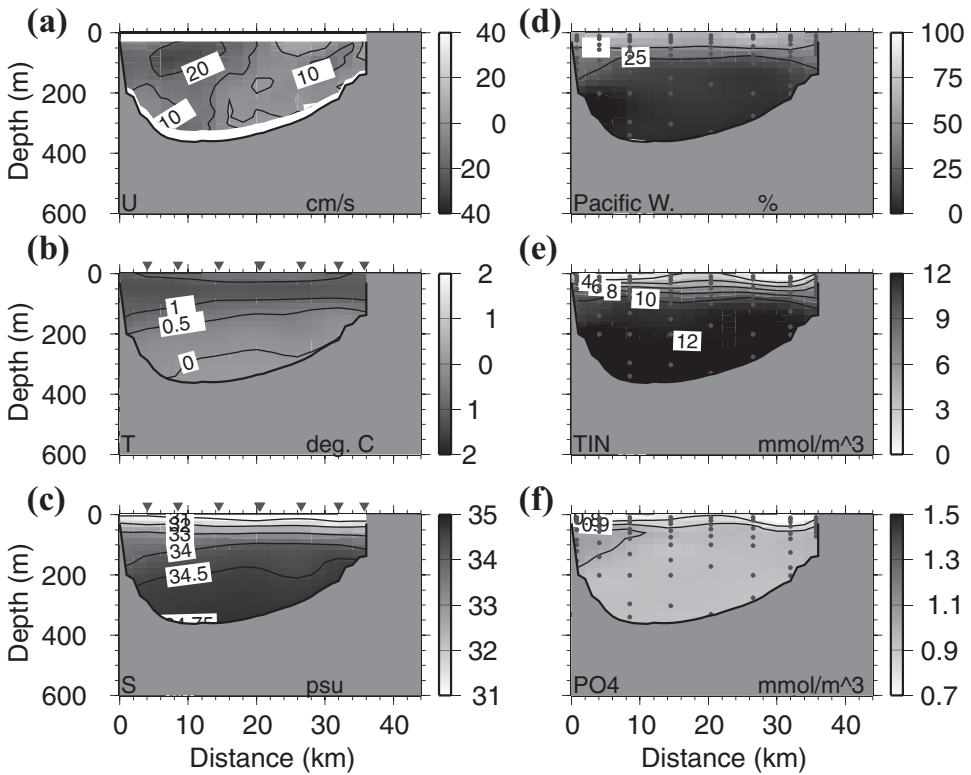
Figure 8. As Figure 6, but for northern Kennedy Channel, i.e., (a) along-channel velocity, (b) potential temperature, (c) salinity), (d) percent Pacific water that is calculated from (e) total inorganic nitrogen (TIN), and (f) phosphate (PO_4) distributions. Symbols indicate hydrographic stations.

The concentrations of dissolved nutrients are highest near 100-m depth within 10-km of Ellesmere Island. The maximum values are lower than in Robeson Channel, probably because tidally forced mixing in the strait has broadened and weakened the core. The highest Pacific-water fraction is above 75% but this isoline, which stretched fully across Robeson Channel, rings a zone that is only 4-km wide by 50-m deep layer in northern Kennedy Channel (Fig. 8) and is absent in the south (Fig. 9).

Integrals across the sections yield net volume fluxes of -0.92 and -0.91 Sv at the northern and southern ends of Kennedy Channel, 19% larger than the value for Robeson Channel (-0.77 Sv; Table 1); however, the along-channel winds opposing these fluxes were 12 m s^{-1} in Robeson Channel while they were 2.5 m s^{-1} in Kennedy Channel during our surveys (Table 1). The fluxes of southward flowing water only are -0.94 Sv and −0.97 Sv for northern and southern Kennedy Channel and −0.96 Sv in Robeson Channel. The differences could reflect day-to-day variations in the flow. Values of the net freshwater flux are -31 and -30 10^{-3} Sv at the northern and southern Kennedy Channel.
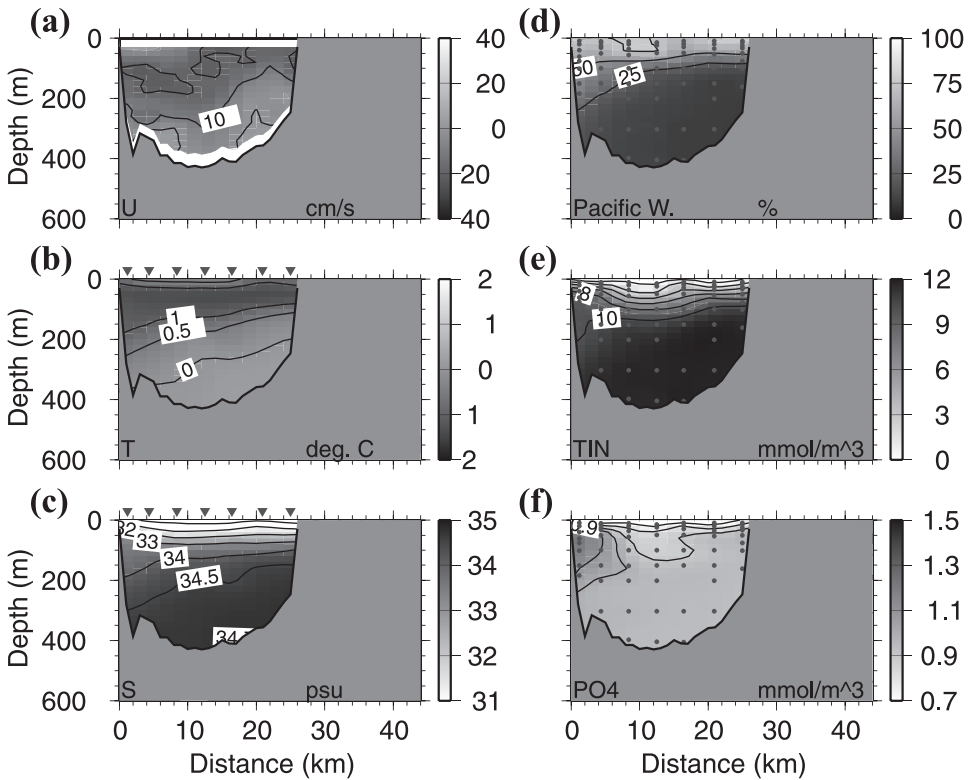
Figure 9. As Figure 6, but for southern Kennedy Channel, i.e., (a) along-channel velocity, (b) potential temperature, (c) salinity), (d) percent Pacific water that is calculated from (e) total inorganic nitrogen (TIN), and (f) phosphate (PO_4) distributions. Symbols indicate hydrographic stations.

d. Cross-sections of Smith Sound

The previously discussed sections lie to the north of the 220-m sill in northern Kane Basin. Our cross-section of Smith Sound is 150 km to the south of the sill where the strait is 45-km wide and 600-m deep. Smith Sound is a short link between two wider water bodies, Kane Basin to the north and Baffin Bay in the south. The cyclonic circulation of water within each basin complicates a simplistic two-dimensional "channel flow" view of Smith Sound. Re-circulation of flow through Smith Sound is likely because its waters shoal to the north, causing depth contours on the Greenland side to curve across and follow the Ellesmere side back south. The data collection in Smith Sound was less systematic than that farther north, being conducted during transit northward on August 2-3 and return on August 14-15. Our results here are less certain because they are derived from a composite of two surveys conducted 12 days apart, each with fewer degrees of freedom than those across Kennedy and Robeson Channel.
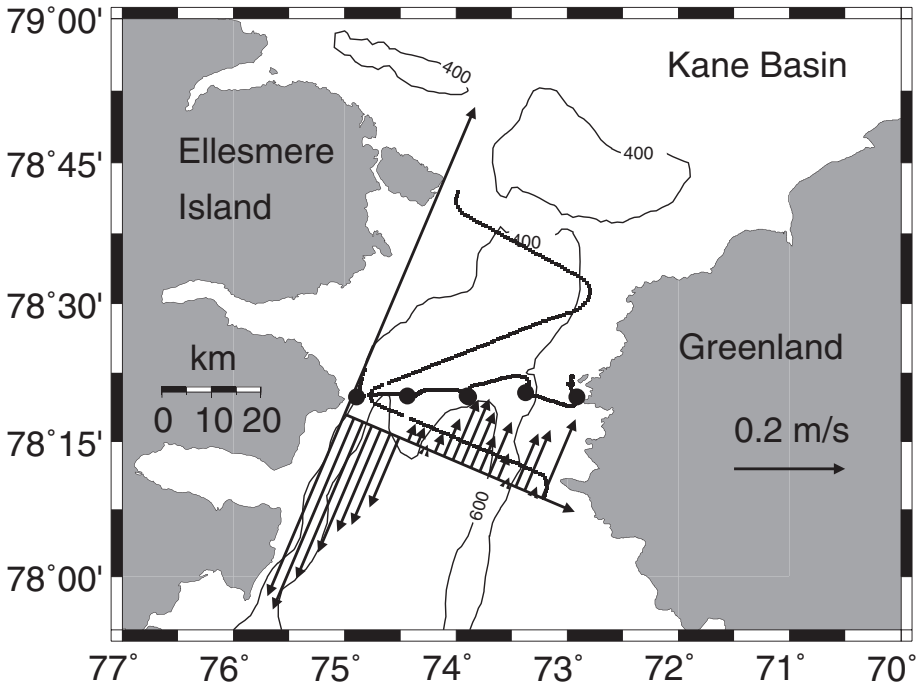
Figure 10. As Figure 4, but for Smith Sound. Small dots indicate ADCP data and large circles
  indicate hydrographic stations. Coordinate systems are indicated by long arrows anchored to a
  coastal point on Ellesmere Island.

Nevertheless, the surveys revealed a narrow strong southward flow within 10 km of
Ellesmere Island (Fig. 10 and Fig. 11). The lateral shear was comparable to that in Robeson
Channel 400 km to the north (Fig. 5). At the Ellesmere coast there was southward flow at
60 cm s^{-1} at the surface, 35 cm s^{-1} at 108-m depth and more than 10 cm s^{-1} at 350 m. The
strength of the latter flow well below sill depth for Nares Strait is indicative of a
recirculation of flow in Kane Basin. The southward stream occupied the western third of
Smith Sound. There was a well- defined northward flow in the eastern half of the section.
The net volume flux was –1.03 Sv with a -1.48 Sv southward component and a 0.45 Sv
northward component. The flux is consistent with the values measured in Kennedy and
Robeson Channels.

Melling *et al.* (2001) have discussed observations of current by instruments moored in
Smith Sound during September 1997 to July 1998. At a location 4.1 km from Ellesmere
Island, the 10-month average flow was southward at 13 cm s^{-1} at 22 m and 16 cm s^{-1} at
100 m, values substantially lower than the 2-day average 35-40 cm s^{-1} at the same location
reported here. At a location 26 km from Ellesmere Island, the average flow was northward
at 4.5 cm s^{-1} at 320 m depth and west-north-west at 1 cm s^{-1} at 490 m. Figure 11 indicates a
3 cm s^{-1} northward flow at the shallower depth at this location. We do not attach much
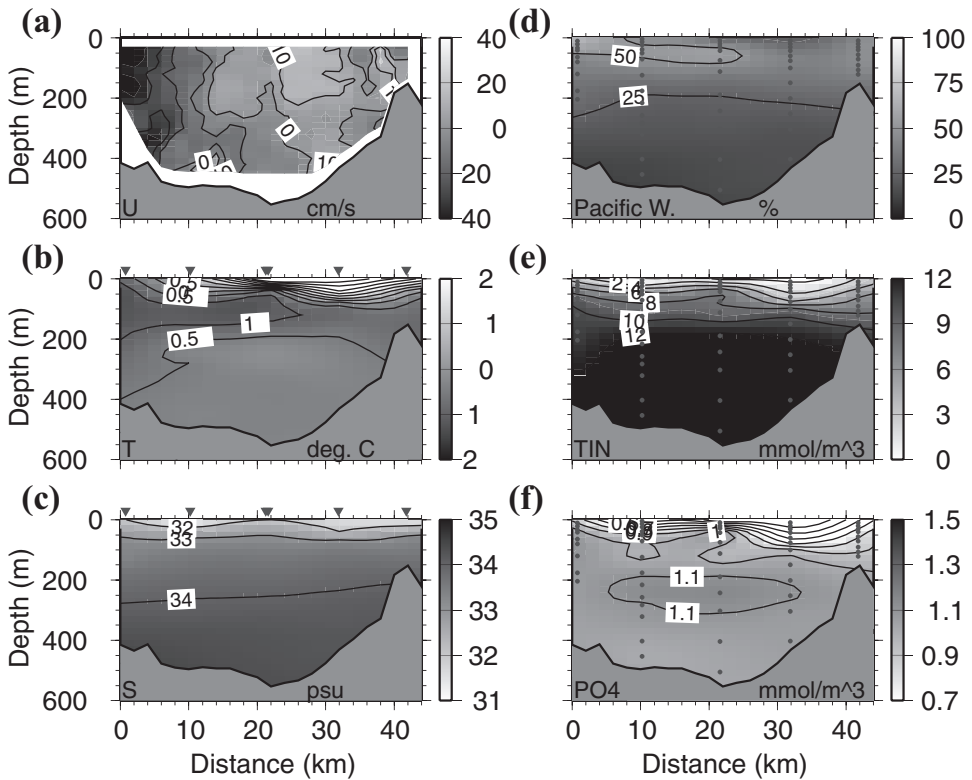
Figure 11. As Figure 6, but for Smith Sound for currents at 108-m depth, i.e., (a) along-channel velocity, (b) potential temperature, (c) salinity), (d) percent Pacific water that is calculated from (e) total inorganic nitrogen (TIN), and (f) phosphate (PO4) distributions. Symbols indicate hydrographic stations.

significance to the apparent changes of velocity or flux estimates. Prior observations represent averages from long mooring records that may not resolve the spatial scales while our observations are a short snapshot in time only; however, our snapshots do resolve spatial scales of variations that mooring records usually do not resolve. In order to provide reliable flux estimates for climate studies, records that resolve both the long time and the short space scales are required.

While the vessel-mounted ADCP resolves a 2-km scale, the 10-km separation of hydrographic stations did not resolve the internal Rossby radius in Smith Sound. Hence the consistency of hydrographic and flow cross-sections cannot be established and comments on nutrient and freshwater fluxes will be tentative. A temperature minimum layer at about -1°C extended about half way across the channel from Ellesmere Island at 100-m depth. Water at and above this layer contained 50% Pacific water while that below the 220-m sill depth contained less that 25% (Fig.11). The isolines of salinity (viz. density) were almost

level and featureless across the sound, indicating that the flows observed were not in geostrophic balance with the cross-channel baroclinic pressure gradient. The predominance of barotropic flow here differs from the situation in Kennedy (Münchow *et al.*, 2006) and Robeson Channels farther north.

4. Summary and conclusions

Our understanding of the influence of Arctic outflows on the meridional overturning circulation is based largely on numerical models. The accumulation of surface freshwater in regions of deep convection and its impact on vertical stratification constitutes the primary mechanism of influence. In the models, freshwater and volume fluxes from high latitudes are parameterized in terms of other model variables or boundary conditions. Empirical testing of these parameterization and boundary conditions is impossible with direct observations. Measurements presented here and in Münchow *et al.* (2006) provide the first empirically constrained estimates (albeit snapshots) of fluxes via Nares Strait. These snapshots do not encompass time variations as the result of variable forcing. The latter is presently under investigation using a three-year time series of observation aquired from an instrumented section in southern Kennedy Channel.

More specifically, our data from ship-based surveys in August 2003 provide the first concurrent descriptions of flow and hydrographic structure in Nares Strait. These reveal property distributions in Nares Strait between its connection to the Arctic Ocean near 83N and that to Baffin Bay near 78N. The velocity measurements are coherent on scales approximately 2 km in the cross-channel coordinate, 100 km in the along-channel and 15 m in depth. These scales are sufficient to realistically map rotationally constrained barotropic and baroclinic flows in Nares Strait as well as associated property fluxes.

The dominant feature of the flow in Nares Strait in 2003 was a southward current that exceeded any counterflow (Fig. 12). Only in southern Smith Sound did we observe substantial recirculation. Most of the southward flux was carried in a narrow (10 km) subsurface jet centered near 100-m depth against the Canadian side of the channel. This feature was present in all sections surveyed. The jet carried a volume flux of 1.09 ± 0.26 Sv that was consistent between sections. Its width was comparable to the internal Rossby radius that commonly scales buoyancy-driven coastal currents (Münchow and Garvine, 1993). The jet ran counter to the prevailing local winds both during our surveys and the weeks preceding them.

There was a northeastward flow along the Greenland side of the strait that averaged 0.18 ± 0.19 Sv in the four sections; there is a suggestion that this counter-flow may have weakened with progression toward the Arctic Ocean, perhaps through re-circulation and mixing with the southward outflow. The net flux of volume was 0.91 ± 0.10 Sv southward averaged over the four cross-sections. Wind observations based on the Samelson *et al.* (2006) model and ship-based sensors both indicate that the net ocean volume flux was in the opposite direction to the local winds during July and early August 2003. The opposing
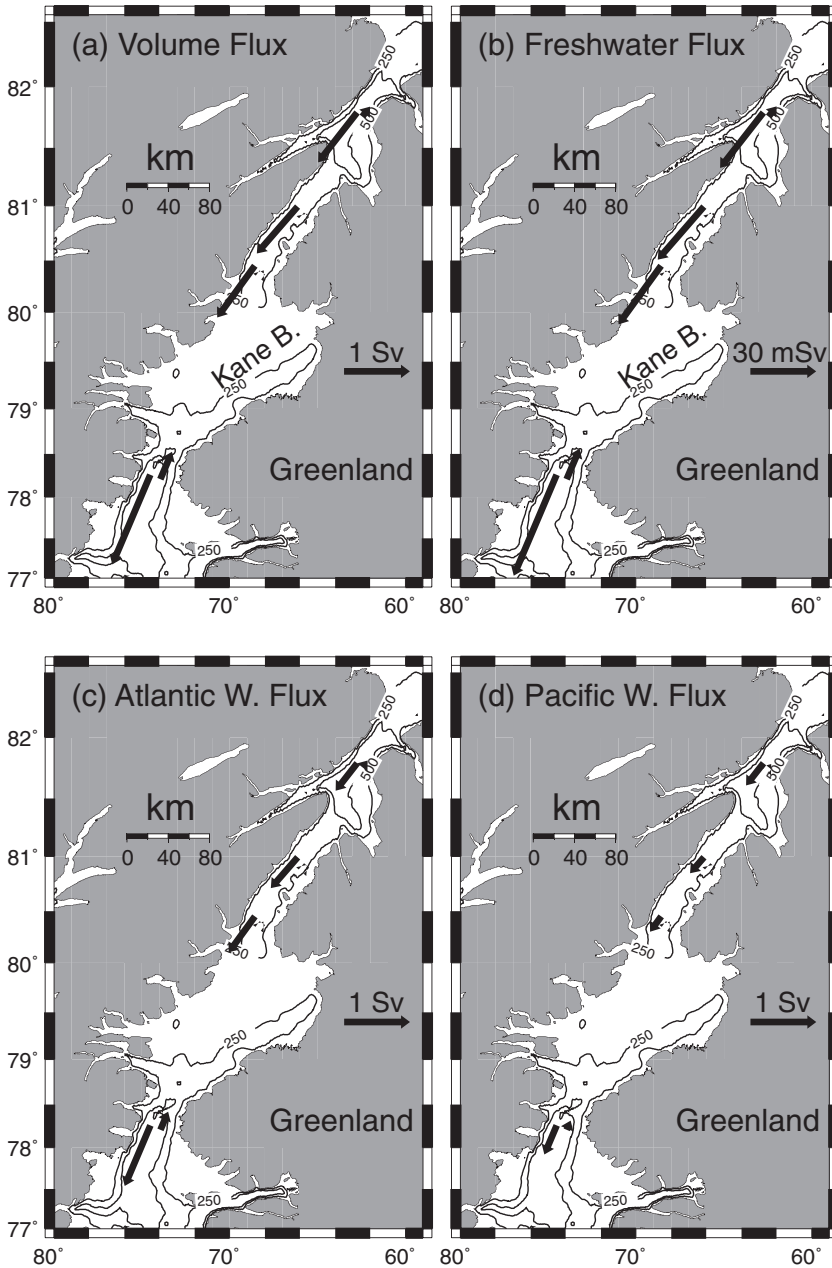
Figure 12. Nares Strait flux of (a) volume, (b) freshwater, (c) Pacific derived water, and (d) Atlantic
    derived water. Contours are bottom depths at 250 m and 500 m. A sill of 220 m is located in
    western Kane Basin near 79.75N latitude.

wind appeared to influence only a 50-m surface layer, slowing the southward current and promoting upwelling on the Ellesmere Island side.

Examining the four estimates of net volume flux in conjunction with along-channel winds during the velocity measurements of each section, we find that the linear regression

$$\text{Flux} = a + b*\text{Wind}$$

gives $a=1.03\pm0.10$ Sv, the volume flux in the absence of a wind, and $b=0.022\pm0.015$ Sv/(m s^{-1}), a wind to volume flux transfer coefficient; uncertainties are at 95% confidence for 2 degrees of freedom. Specifically, the 12 m/s northward wind in Robeson Channel apparently reduced the southward volume flux by about 0.22 Sv from that during observations in Smith Sound when the northward winds were only 2 m/s (Table 1). A linear regression for the freshwater fluxes against wind yields a quiescent value of $34\pm3.4\times10^{-3}$ Sv (1070 ± 107 km^3 y^{-1}) and a transfer coefficient of $0.73\pm0.51\times10^{-3}$ Sv/ (m s^{-1}). Local along-channel winds thus can explain the observed section to section flux variations (Table 1).

Concurrent measurements of geochemical tracers in sampled seawater (inorganic nitrogen and phosphate) permitted the discrimination of Atlantic- and Pacific-derived waters in the through-flow. Pacific water comprised between 75% (Robeson Channel) and 50% (Smith Sound) of surface waters. About 39% or 0.43 ± 0.10 Sv of the southward flowing waters were of Pacific origin. The highest fraction of Pacific water appeared within the strong southward jet adjacent to Ellesmere Island. We thus conclude that the Pacific was the main source for the southward freshwater flux of about $31\pm4\times10^{-3}$ Sv or 977 ± 127 km^3/year (relative to a salinity of 34.8 psu). This value is about a half of the Pacific freshwater inflow through Bering Strait (Woodgate and Aagaard, 2005). Falkner *et al.* (2006) noted that the flow of Pacific water through the Nares Strait is likely subject to strong interannual variation, being higher in 1997 than in 1977 and 2003.

We propose that the southward flux is associated with barotropic and baroclinic adjustment to pressure gradients. Münchow *et al.* (2006) found that 1/3 of the transport through Nares Strait was barotropic and 2/3 baroclinic using the thermal wind balance and direct velocity observations as reference. The barotropic component is likely driven by a drop in total hydrostatic pressure between the Lincoln Sea and Baffin Bay while the baroclinic component is in thermal wind balance with an across-channel density gradients reflecting the presence of cold, fresh Arctic water near the sea surface adjacent to Ellesmere Island and warmer, saltier water at depth and adjacent to Greenland. The dominant baroclinic flow forces a coastally trapped boundary current.

The southward flowing boundary current observed in August 2003 on the western side of Nares Strait ran counter to upwelling-favorable wind. At the surface, the influence of wind apparently overpowered that of current and very little pack was drawn into Nares Strait from the Lincoln Sea. This situation was unusual. In August 2006 and 2007 the local wind was generally downwelling favorable along Ellesmere Island and this condition sustained a fast-moving stream of dense multi-year pack ice from the Lincoln Sea and

likely induced southward current stronger than reported here. The boundary current would be trapped more distinctly at the coast because surface stress and buoyancy act in unison with downwelling-favorable wind.

Pack ice of the Lincoln Sea is the oldest and thickest in the Arctic Ocean. At the steady speed of 0.5 m s^{-1}, which apparently prevailed in August of both 2006 and 2007, such ice could reach Baffin Bay in about 10 days. For an assumed 4-m thichness and 5-10 tenths concentration within a 10-km wide stream, the ice-associated freshwater flux would be $10-20 \times 10^{-3}$ Sv, a value equal to about half the oceanic freshwater flux and much larger than the 3×10^{-3} Sv estimated as a long-term 1996-2002 average estimated from RADAR-SAT (Kwok, 2005). We attribute the discrepancy to the typical formation of landfast ice in Nares Strait for between 3-7 months each winter (Agnew, 1998; Kwok, 2005), when no ice flux occurs. When stabilizing ice bridges anchored to land fail to form, such as during the winter of 2006/07, the coastal current along Ellesmere Island that transports about 30×10^{-3} Sv of oceanic freshwater year-round may also advect an additional 10×10^{-3} Sv of freshwater in the form of ice southward. How all this buoyancy is distributed in the Baffin Bay and the Labrador Sea is an open question that merits future study.

Serreze *et al.* (2006) synthesized terrestrial, atmospheric, and oceanographic observations and model results to estimate a freshwater budget for the Arctic Ocean. They estimated that 35% of the total liquid freshwater export from the Arctic passes through the Canadian Archipelago, a value derived from two moorings yielding a 6-year time series in Lancaster Sound (Prinsenberg and Hamilton, 2005). Their estimates for this 68-km wide channel are 0.70 Sv for volume and 48×10^{-3} Sv for freshwater flux. For Nares Strait, we estimate fluxes in the absence of wind influence to be 1.03 ± 0.10 Sv for volume and $34 \pm 3 \times 10^{-3}$ Sv for freshwater. At present, unfortunately, the Nares Strait values are not derived from long-term data and the Lancaster Sound values are not derived from spatially resolved data. Discarding these limitations, it appears that (a) each of these pathways contributes substantially to volume and freshwater fluxes, (b) combined they export as much freshwater as enters the Arctic Ocean via Bering Strait, (c) combined they carry as much oceanic freshwater from the Arctic as the East Greenland Current (Serreze *et al.*, 2006), and (d) each contributes about the same freshwater flux as the East Greenland Coastal Current described by Bacon *et al.* (2002) which appears to form on the shelf off the southern tip of Greenland within an internal deformation radius of the coast.

Our ship-based velocity surveys provide evidence of the importance of the internal Rossby radius of deformation (only about 10 km in Arctic outflows) to the transport of oceanic buoyancy such as freshwater. Since arrays of oceanographic moorings rarely resolve the flow close to this spatial scale of variability, many published estimates of oceanic flux are sensitive to the perhaps arbitrary choice of computational weights assigned to each instrument's measurements for integration of flow over a cross-section. Our results, albeit limited in time, provide important physical insights for the interpretation of data from moored instruments and for the realistic assignment of computational weights (and their uncertainty) when using sparsely instrumented arrays.

Accurate estimates of volume and freshwater fluxes throught the Canadian Archipelage are, however, only one aspect of control on the global meridional circulation. The manner in which coastall trapped freshwater fluxes are mixed into the adjacent deep basin of the Labrador Sea, where they can influence vertical stratification in regions of deep convection, is still unresolved.

APPENDIX

a. Processing and screening of data from the ship-mounted ADCP

Data acquired by ship-mounted ADCP, particularly on icebreakers, may be contaminated by the presence of ice, bubbles and high ambient noise. For this reason, we recorded data for every ping, so that values could be carefully screened before ensemble averaging to reduce sampling error. The reduction in error variance via averaging is based on the assumption that the Doppler shift is a Gaussian variable.

We tested this assumption by comparing the ensemble mean and the ensemble median of Doppler velocity, which are the same for a Gaussian variable. In these data a large difference between these two statistics was common, even in cases where the data fell within the tolerance bounds for error velocity, a common criterion for quality control (e.g. VMDAS, the RDI data collection and processing software). Only a very restrictive tolerance on error velocity was equally effective, and this removed a large fraction of valid data.

Our processing followed this sequence. Convert Doppler speed from each ping in the direction of each beam into an earth-referenced vector by applying heading, pitch and roll information, calibration coefficients and ship's absolute velocity. Sort the values during each averaging interval (the ensemble) in order of magnitude. Remove the largest and smallest tenths of the data on the assumption that invalid data yield values at the extremes of the observed range; we have used only 80% of the values, those in the middle of the observed range. The removal of extreme values from the record effectively forces our data distribution toward a Gaussian distribution for which the standard deviation is a more useful metric than that from an ensemble including outliers.

Following each water-tracking pulse, the ADCP transmitted a bottom-tracking pulse to determine the ship's velocity relative to the seabed. It is necessary to subtract the latter

vector from current vector measured relative to the ship to derive current relative to the Earth. The selection of acceptable bottom-track data followed the same procedure described for water-column values. Seabed echoes yield the most accurate measure of the ship's movement. Where water was too deep for bottom tracking, deeper than 1000 m, the p-code differential Global Position System (DGPS) aboard the USCGC *Healy* provided an alternate source of ship's velocity.

Because the water-column and bottom-track velocities were derived by the same instrument, a comparison of the ship's velocity from navigational DGPS and bottom-tracking allowed an evaluation of the ADCP's calibration (Joyce, 1989). Figure A1a displays histograms of the difference between DGPS and ADCP derived east and north velocity components, which typically range over ± 8 m s^{-1}. The graphs reflect the combined inaccuracies of the Doppler sonar, of the heading pitch and roll sensors, of the navigational GPS and of the data processing algorithms for quality control and calibration. Based on cumulative histograms (Fig. A1b) we conclude that within a 2-minute interval, 90% of the velocity values agree to within ± 0.08 m s^{-1}, about 1% of the actual value. Since the histograms are symmetric and Gaussian in shape, we note that averaging (in space or time) will reduce uncertainty in proportion to $1/\sqrt{N}$, where N is the number of data averaged. We have taken advantage of averaging in the preparation of the composite cross-sections of along-channel flow.

b. Tides

Tides provide the dominant component of current in Nares Strait. Their signal must be removed from cross-sections of flow acquired by vessel-mounted ADCP over relatively short times in order to reveal subtidal circulation. Tidal currents in Nares Strait are barotropic, deterministic and predictable (Münchow *et al.*, 2006; Padman and Erofeeva, 2004). However, the amplitudes and phases of tidal constituents vary substantially both along and across the strait. We have used the tidal model of Padman and Erofeeva (2004) to predict the tidal current at the time and location of observation by ADCP, and have used the predictions to remove much of the tidal oscillation from the data. Münchow *et al.* (2006) evaluate this approach by comparing modeled tidal currents with a set of least square data fitting procedures using ADCP-derived velocities.

Figure A2 shows predicted tidal currents and depth-averaged, band-filtered along-channel tidal current measured by the ADCP at a location closest to Ellesmere Island (see Fig. 1) during the period of observation in August 2003. For the three-year record (not shown), more than 94% of the observed variance is correlated with the modeled current; the root-mean-square residual is 4.7 cm s^{-1}. Discrepancies between actual and predicted tidal currents are further reduced by the compositing of sections described in the next section.

c. Spatial averaging

ADCP data were collected opportunistically as the ship moved in support of various scientific activities (hydrographic stations, mooring deployments, seabed survey, piston
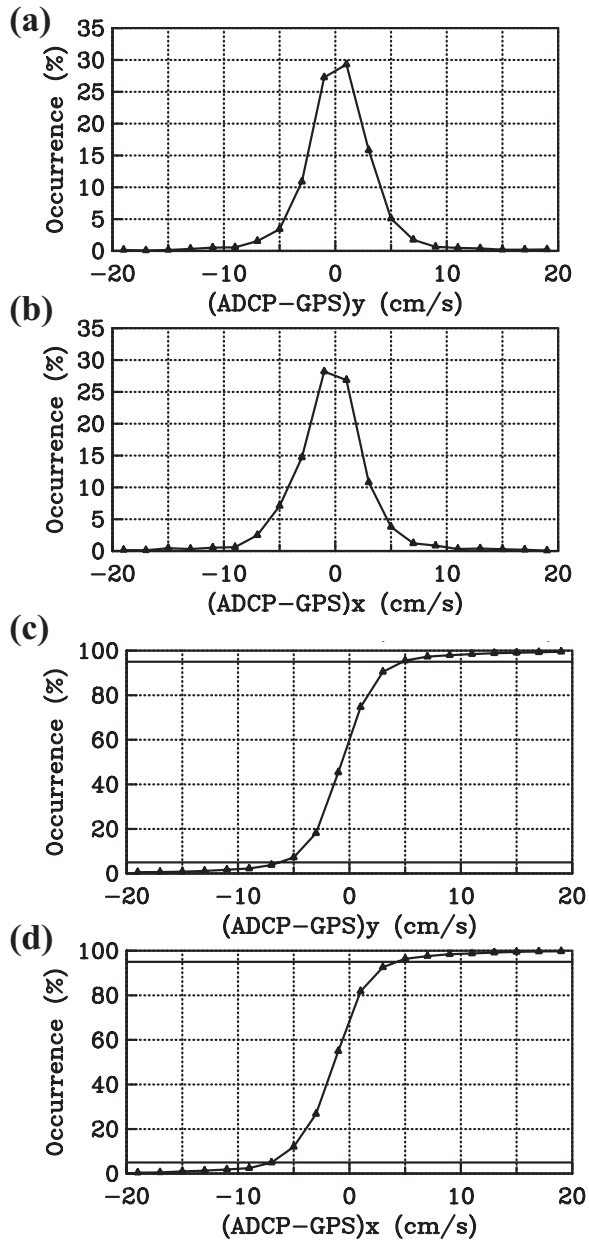
Figure A1. Differences of vessel-mounted ADCP and DGPS derived ship's velocity vector compo-
nents as (a) histogram north, (b) histogram east, (c) integrated histogram north and (d) integrated
histogram east for a one minute ensemble average. The solid lines in (c) and (d) represent 5% and
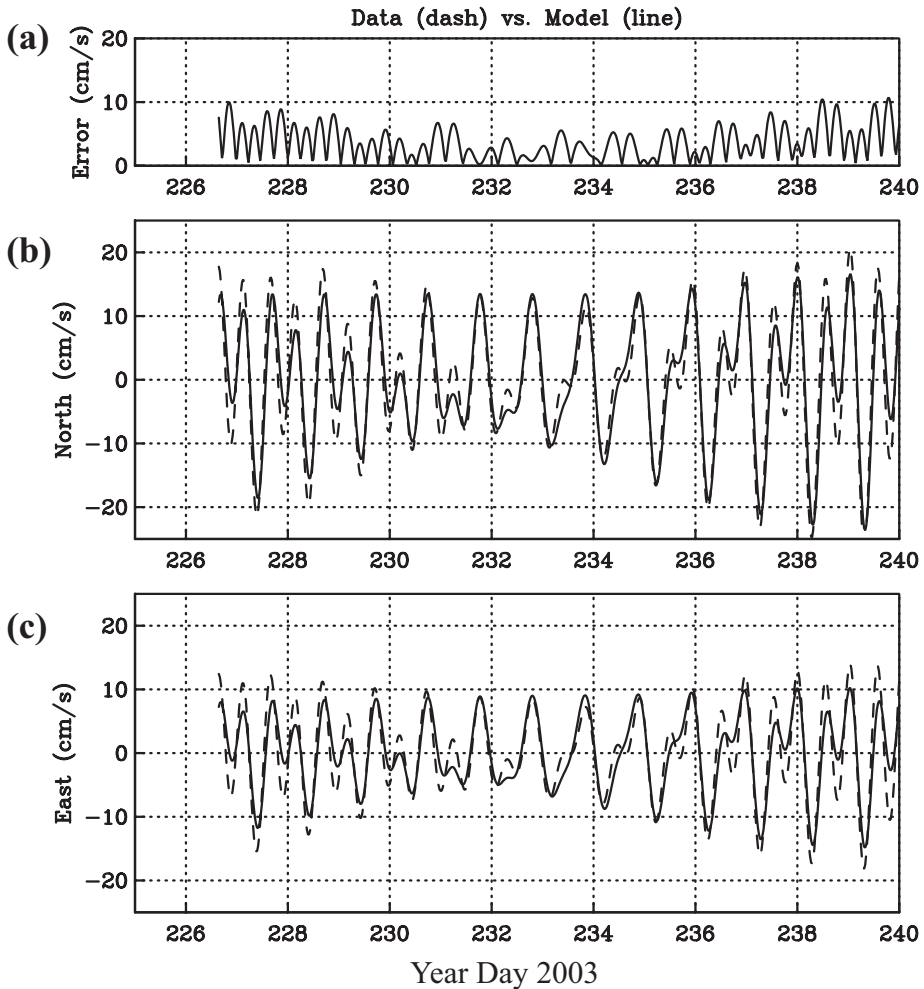95% confidence limits.

Figure A2. Comparison of depth-averaged, band-pass filtered, tidal velocity time series from KS-02 mooring data (dash) against model predictions (solid line): (a) discrepancy in speed (rms~4.7 cm s^{-1}), (b) north, and (c) velocity components. About 94% of the observed tidal variance is correlated with the modeled tidal variance (r^2~0.94).

coring). In order to project the velocity data collected along a meandering path within a study area onto reference sections, we have defined local coordinate systems at four positions along the strait. We have mapped the ship's location and the de-tided current data acquired in the vicinity of each reference section into along and cross channel components and have then averaged values within 2-km wide cross-channel bins. Through such averaging, the inherent instrument, tidal and environmental noise in subtidal currents has been reduced.

d. Extrapolation to the surface

The vessel-mounted ADCP system does not return useful data within about 18.5 m of the surface on account of the 8.5 m draft of the vessel and a 10-m blanking interval for the transducers to ring down. Using a 15-m vertical bin size, the center of our first velocity recording is nominally located about 26 m below the sea surface. Potentially a substantial fraction of the freshwater flux may reside within this surface layer on account of its generally low salinity measurements. Rather than ignoring this layer we here fit velocity observations over the top 100 m of the water column to an Ekman layer profile overlaid with a constant shear, e.g.,

$$u(z) = u_0 + u_1^* z + v_E^* s(z) + u_E^* c(z)$$

$$v(z) = v_0 + v_1^* z + v_E^* c(z) - u_E^* s(z)$$

where z is the vertical distance from the surface scaled by the vertical Ekman layer depth $D = (2*A_v/f)^{1/2}$, f is the Coriolis parameter, and A_v is the vertical eddy viscosity, while $s(z) = \sin(z)*e^z$ and $c(z) = \cos(z)*e^z$ are the functions to describe the Ekman layer profile. The 6 free parameters (u_0, v_0), (u_1, v_1), and (u_E, v_E) are to be determined by minimizing the least squares for each vertical velocity profile after all other processing steps have been applied (2-minute temporal averaging, detiding, and averaging into 2-km across-channel bins). Note that along channel u and across-channel v velocity are fitted concurrently, that is, u and v are coupled via the Ekman surface velocity vector (u_E, v_E). The degrees of freedom (dof) thus are dof=2*N-6 where velocity vector estimates from 26 m to 101 m give N=6 data points. The assumed Ekman depth of 50-m corresponds to a vertical eddy viscosity $A_v = 0.18$ m^2 s^{-1} at a latitude of 80.5N and may perhaps be considered too large, however, in the absence of any turbulence or high-resolution surface measurements this depth ensures that some of our velocity observations are within this Ekman layer. Figure A3 shows two profiles from Robeson Channel with the data and the extrapolating fit overlaid for a best and a worst case with 0.4 cm s^{-1} and 2.1 cm s^{-1} uncertainty, respectively. We estimate these uncertainties from the sum of squared differences between measured and fitted velocity components, ε^2, as $1.96*(\varepsilon^2/N/dof)^{1/2}$. While the fit is physically motivated and appears to reproduce the observations well, the implied surface stress is not always dynamically consistent with underway wind observations. More specifically, maximum correlations between surface Ekman velocity (u_E, v_E) and the wind vector are expected to occur at 45° angle, however, here they occur at 85°, 51°, 91° degrees to the right of the wind for Robeson, northern Kennedy, and southern Kennedy Channels. Furthermore, the correlations are weak, i.e., 0.20, 0.44, and 0.22 at the three northern sections. Table A1 summarizes the sensitivity of net volume and freshwater flux estimates to a range of Ekman layer depths. The surface extrapolation adds about 10% to the net fluxes observed below 30 m.

All hydrographic measurements originate from discrete bottle samples with a near-surface bottle located 10 m below the surface. We compare these accurate, single point,
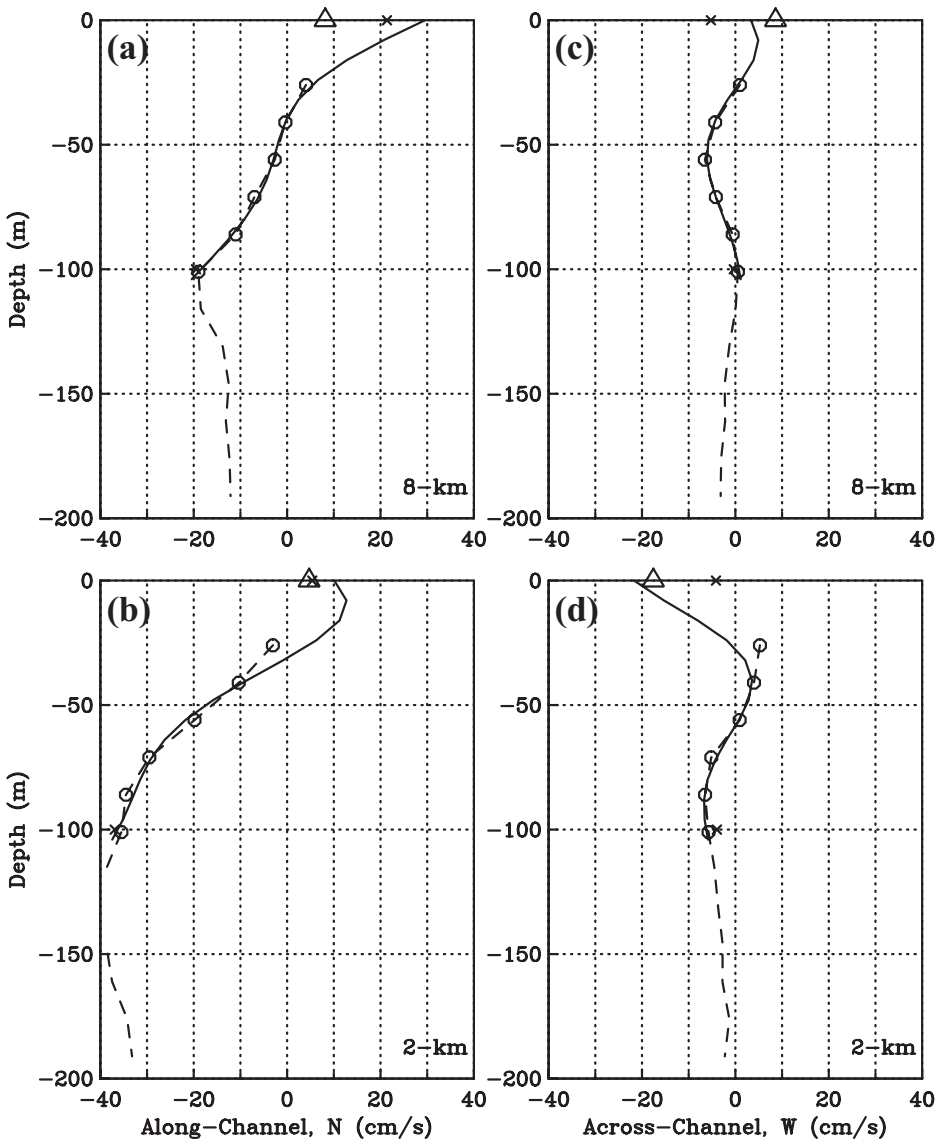
Figure A3. Velocity profiles (dashed line and symbols) from ADCP and least square fit (solid line) for along-channel (left panels, a and b) and across-channel (right panel, c and d) components for Robeson Channel 2-km (bottom, b and d) and 8 km (top, a and c) from the Ellesmere Island coast. The triangle at the surface indicates fitted surface Ekman velocities (u_E, v_E) while crosses represent fitted mean and shear velocities. The circles represent the N=6 velocity observations used to determine the fitted parameters.

Table A1. Sensitivity of flux estimates to Ekman layer depth (Kennedy-S).

Ekman layer depth (m)	Net volume flux (Sv)	Net freshwater flux (10^{-3} Sv)	Angle to wind stress	Correlation to wind stress
10	−0.81	−27.3	−174	0.26
30	−0.93	−31.1	+46	0.17
50	−0.91	−30.4	−91	0.22
75	−0.88	−29.6	−168	0.24
100	−0.87	−29.2	+151	0.24
No extrapolation	−0.80	−27.1		

salinity measurements with salinity estimates from an underway thermosalinograph connected to a water intake located 8 m below the surface. The underway data sampling is similar to that of the ADCP (about 0.25 Hz) and the data from this system are averaged in space similar to the ADCP data. For Robeson Channel we find the averaged underway salinity to be 0.06±0.20 psu lower than the bottle salinity where the uncertainty is a 95% confidence limit based on N=5 samples. Hence we feel justified to ignore vertical stratification of hydrographic properties within the top 10-m of the water column, thus extrapolate the 10-m bottle salinities to the surface for flux calculations.

REFERENCES

Aagaard, K. and E. C. Carmack. 1989. The role of sea ice and other fresh water in the Arctic circulation. J. Geophys. Res., *94*, 14485-14498.

Agnew, T. 1998. Drainage of multi-year sea ice from the Lincoln Sea. Can. Meteor. Oceanogr. Soc. Bull., *26*, 101-103.

Bacon, S., G. Reverdin, I. G. Rigor and H. M. Snaith. 2002. A freshwater jet on the east Greenland shelf. J. Geophys. Res., *107*, doi:10.1029/2001JC000935.

Belkin, I. M., S. Levitus, J. Antonov and S.-A. Malmberg. 1998. "Great Salinity Anomalies" in the North Atlantic. Prog. Oceanogr., *41*, 1-68.

Bryden, H. L., H. R. Longworth and S. A. Cunningham. 2005. Slowing of the Atlantic meridional overturning circulation at 25°N. Nature, *438*, 655-657.

Curry, R. and C. Mauritzen. 2005. Dilution of the northern North Atlantic in recent decades. Science, *308*, 1772-1774.

Delworth, T. H. and K. W. Dixon. 2000. Implication of recent trends in the Arctic/North Atlantic oscillation for the North Atlantic thermohaline circulation. J. Climate, *13*, 3271-3727.

Dickson, R., J. Lazier, J. Meincke, P. Rhines and J. Swift. 1996. Long-term coordinated changes in the convective activity of the North Atlantic. Prog. Oceanogr, *38*, 241-295.

Dickson, R. R., T. J. Osborn, J. W. Hurrell, J. Meincke, J. Blindheim, B. Adlandsvik, T. Vinje, G. Alekseev and W. Maslowski. 2000. The Arctic Ocean response to the North Atlantic Oscillation. J. Climate, *13*, 2671-2696.

Dickson, B., I. Yashayaev, J. Meinke, B. Turrell, S. Dye and J. Holfort. 2002. Rapid freshening of the deep North Atlantic over the past four decades. Nature, *416*, 832-837.

Dickson, R. R., S. Dye, M. Karcher, J. Meincke, B. Rudels and I. Yashayaev. 2007. Current estimates of freshwater flux through Arctic ands seas. Prog. Oceanogr., *73*, 210-230.

Falkner, K. K., M. C. O'Brian, H. Melling, E. C. Carmack, A. Münchow and E. P. Jones. 2008.

Interannual variability of dissolved nutrients in the Canadian Archipelago and Baffin Bay with implications for freshwater flux. J. Geophys. Res. (submitted).

Godin, G. 1979. Currents in Robeson Channel, Nares Strait. Mar. Geod., *2*, 351-364.

Gordon, L. I. *et al.* 1994. A suggested protocol for continuous flow automated analysis of seawater nutrients (phosphate, nitrate, nitrite and silicic acid) in the WOCE Hydrographic Program and the Joint Global Ocean Fluxes Study. WOCE Operations Manual, Vol. 3: The Observational Programme, Section 3.1: WOCE Hydrographic Programme, Part 3.1.3: WHP Operations and Methods., WHP Office Report WHPO 91-1, 52 loose-leaf pp., Woods Hole, MA.

Hendrik, H. 1878. Memoirs of Hans Hendrik, the Arctic traveller, serving under Kane, Hayes, Hall and Nares, 1853-1876, trans. H. J. Rink, ed. George Stephens, Trübner and Co., London.

Johnson, H. L. and C. Garrett. 2006. What fraction of a Kelvin wave incident on a narrow strait is transmitted? J. Phys. Oceanogr., *36*, 945-954.

Jones, E. P., L. G. Anderson and J. H. Swift. 1998. Distribution of Atlantic and Pacific waters in the upper Arctic Ocean: Implications for circulation. Geophys. Res. Lett., *25*, 765-768.

Jones, E. P. and A. J. Eert. 2006. The waters of Nares Strait in 2001. Polarforschung, *74*, 185-189.

Joyce, T. M. 1989. On the *in situ* calibration of shipboard ADCPs. J. Atmos. Ocean. Tech., *6*, 169-172.

Kwok, R. 2005. Variability of Nares Strait ice flux. Geophys. Res. Lett., *32*, C01009, doi:10.1029/2003JC001785.

Melling, H. 2000. Exchange of freshwater through the shallow straits of the North American Arctic, *in* The Freshwater Budget of the Arctic Ocean, E.L. Lewis *et al.*, eds., Kluver Academic Publishers, Dortdrecht, Netherlands, 479-502.

Melling, H., Y. Gratton and G. Ingram. 2001. Ocean circulation within the North Water Polynya of Baffin Bay. Atmos. Oceans, *39*, 301-325.

Münchow, A. and R.W. Garvine. 1993. Buoyancy and wind forcing of a coastal current. J. Mar. Res., *51*, 293-322.

Münchow, A., H. Melling and K. K. Falkner. 2006. An observational estimate of volume and freshwater fluxes in Nares Strait. J. Phys. Oceanogr., *36*, 2025-2041.

Nutt, D. C. 1966. The drift of Ice Island WH5. Arctic, *19*, 244-262.

Padman, L. and S Erofeeva. 2004. A barotropic inverse tidal model for the Arctic Ocean. Geophys. Res. Lett., *31*, doi:10.1029/2003GL019003.

Prinsenberg, S. J. and J. Hamilton. 2005. Monitoring the volume, freshwater, and heat fluxes passing through Lancaster Sound in the Canadian Archipelago. Atmos. Oceans, *43*, 1-22.

Rahmstorf, S. and A. Ganopolski. 1999. Long-term global warming scenarios computed with an efficient coupled climate model. Climate Change, *43*, 353-367.

Rhein, M., J. Fischer, W. M. Smethie, Jr., D. Smythe-Wright, R. F. Weiss, C. Mertens, D.-H. Min, U. Fleischmann and A. Putzka. 2002. Labrador Sea Water: Pathways, CFC - Inventory and Formation Rates. J. Phys. Oceanogr., *32*, 648-665.

Sadler, H. E. 1976. Water, heat and salt transports through Nares Strait, Ellesmere Island. J. Fish. Res. B. Can., *33*, 2286-2295.

Samelson, R. M., T. Agnew, H. Melling and A. Münchow 2006. Evidence for atmospheric control of sea-ice motion through Nares Strait. Geophys. Res. Lett., *33*, L02506, doi:10.1029/2005GL025016.

Samelson, R. M. and P. L. Barbour. 2008. Low-level winds, orographic effects and extreme events in Nares Strait, a model-based mesoscale climatology. Mon. Weather Rev. (in press).

Serreze, M. C., A. P. Barrett, A. G. Slater, R. A. Woodgate, K. Aagaard, R. B. Lammers, M. Steele, R. Moritz, M. Meredith and C. M. Lee. 2006. The large-scale freshwater cycle of the Arctic. J. Gephys. Res., *111*, doi:10.1029/2005JC003424.

Taylor, J. R., K. K. Falkner, U. Schauer and M. Meredith. 2003. Quantitative consideration of

dissolved barium as a tracer in the Arctic Ocean. J. Geophys. Res., *108*, doi:10.1029/2002JC001635.

Vellinga, M. 2005. Sensitivity of the MOC to vertical distribution of freshwater pertubations. ASOF Newsletter, *3*, 18-20.

Weaver, A. J., S. M. Aura and P. G. Myers. 1994. Interdecadal variability in an idealized model of the North Atlantic. J. Geophys. Res., *99*, 12423-12441.

Wohlleben, T. M. H. and A. J. Weaver. 1995. Interdecadal climate variability in the subpolar North Atlantic. Clim. Dynam., *11*, 459–467.

Woodgate, R. A. and K. Aagaard. 2005. Revising the Bering Strait freshwater flux into the Arctic Ocean. Geophys. Res. Lett., *32*, L02602, doi:10.1029/2004GL021747.

Wunsch, C. and P. Heimbach. 2006. Estimated decadal changes in the North Atlantic meridional overturning circulation and heat flux 1993–2004. J. Phys. Oceanogr., *36*, 2012-2024.

Yamamoto-Kawaii, M., F. A. McLaughlin, E. C. Carmack, S. Nishino and R. Shimada. 2008. Freshwater budget of the Canada Basin, Arctic Ocean from salinity, ä^{18}O, and nutrients. J. Geophys. Res., *113*, doi: 10.1029/2006JC003858,2008.

Zweng, M. and A. Münchow. 2006. Warming and freshening of Baffin Bay, 1916-2003. J. Geophys. Res., *111*, C07016, doi:10.1029/2005JC003093.